Bioactive Materials 6 (2021) 1040–1050

Contents lists available at ScienceDirect

Bioactive Materials

journal homepage: http://www.keaipublishing.com/biomat

Intelligent H2S release coating for regulating vascular remodeling

Bingyang Lu[a,b,1], Xiao Han[a,b,1], Ansha Zhao[a,b,*], Dan Luo[a,b], Manfred F. Maitz[c], Haohao Wang[a,b], Ping Yang[a,b], Nan Huang[a,b]

[a] Key Laboratory of Advanced Technologies of Materials, Ministry of Education, Southwest Jiaotong University, Chengdu, 610031, China
[b] School of Materials Science and Engineering, Southwest Jiaotong University, Chengdu, 610031, China
[c] Leibniz-Institute of Polymer Research Dresden, Max Bergmann Center of Biomaterials Dresden, Hohe Strasse 6, 01069, Dresden, Germany

ARTICLE INFO

Keywords:
pH responsive
Layer-by-layer self-assembly film
H_2S
Coronary atherosclerosis

ABSTRACT

Coronary atherosclerotic lesions exhibit a low-pH chronic inflammatory response. Due to insufficient drug release control, drug-eluting stent intervention can lead to delayed endothelialization, advanced thrombosis, and unprecise treatment. In this study, hyaluronic acid and chitosan were used to prepare pH-responsive self-assembling films. The hydrogen sulfide (H_2S) releasing aspirin derivative ACS14 was used as drug in the film. The film regulates the release of the drug adjusted to the microenvironment of the lesion, and the drug balances the vascular function by releasing the regulating gas H_2S, which comparably to NO promotes the self-healing capacity of blood vessels. Drug releasing profiles of the films at different pH, and other biological effects on blood vessels were evaluated through blood compatibility, cellular, and implantation experiments. This novel method of self-assembled films which H_2S in an amount, which is adjusted to the condition of the lesion provides a new concept for the treatment of cardiovascular diseases.

1. Introduction

Intervention therapy is the most commonly used treatment for atherosclerotic stenoses. This method is less traumatic, less risky, has a quick recovery, and is effective in clinical practice. However, an atherosclerotic lesion provides a complex pathophysiological environment, including a low pH, high oxidative stress, and chronic inflammation [1]. An interventional treatment inevitably causes damage to local tissues, leading to complications such as inflammation, intimal hyperplasia, late thrombosis, and in-stent restenosis [2,3]. The emergence of drug-eluting stents, which release drugs at the site of the lesion was a revolutionary development in the field of interventional therapies. Usually, drugs such as paclitaxel [4] and rapamycin [5] for inhibition of tissue proliferation, heparin [6] to prevent blood clotting and thrombosis, or VEGF [7] (vascular endothelial growth factor), which supports neovascularization, are used. However, most drug-loaded stents show burst release after implantation, which causes non-satisfying over-und underdosing over time. Moreover, clinically used anticancer drugs, paclitaxel [8] and rapamycin [9], inhibit the proliferation of various cell types, including the endothelial cells, what limits the success in interventional therapy. In the early stages, it can inhibit intimal hyperplasia, prevent inflammation, and restenosis. However, even after the effect of the drug diminishes, the new blood vessels do not completely heal, leading to further complications. In addition, the commonly used stent material, polylactic acid produces acidic degradation products, which causes local acidosis [10,11]. Therefore, materials with better biocompatibility are needed. In summary, currently, there are several challenges related to the biocompatibility of the materials used for stents and stent coatings, the effects of stent and loaded drugs on biological systems, and the controlled release of the drugs from the coatings in vascular disease intervention therapies.

Current drug-carrying stents are primarily either drug-eluting or degradable polymers. Drug-eluting stents are implaned with the drug loaded within the polymer coating or directly on the surface of the stent, and these stents have not the ability to intelligent drug release. Seo et al. [12] used biocompatible polyurethane to make films which could be loaded with the lipophilic drug paclitaxel drugs. Polyethylene glycol (PEG) incorporated as a pore forming agent, varying amounts of PEG resulted in different degrees of porosity, which allowed tailoring

Peer review under responsibility of KeAi Communications Co., Ltd.
* Corresponding author. Key Lab. for Advanced Technologies of Materials, Ministry of Education, School of Material Science and Engineering, Southwest Jiaotong University, Chengdu, 610031, PR China.
E-mail address: anshazhao@263.net (A. Zhao).
[1] First author; Bingyang Lu and Xiao Han, We declare that Bingyang Lu and Xiao Han have the same contribution for the paper.

https://doi.org/10.1016/j.bioactmat.2020.09.023
Received 15 May 2020; Received in revised form 20 August 2020; Accepted 26 September 2020

the rate of drug release. Most of the studies highlight the drug release capability of degradable polymer scaffolds [13,14]; hence, a drug release model of degradable polylactic acid scaffold was established [15]. These scaffolds rely primarily on the degradation of the polymer to prevent burst release of the drug. The development of nanoparticles, which are loaded onto the scaffold provided a flexible strategy for sustained release of drugs by loading polymer micelles onto a scaffold gel network [16] or by promoting the adsorption of the micelles on the surface of the stent by electrostatic interactions [17]. However, a controlled release of the drugs adapted to the condition of the microenvironment of the lesion for a precise and personalized treatment is difficult to achieve. A feedback-control anticoagulant release system with coagulation-triggered heparin release has been suggested elsewhere [18,19]. Ideally, the implanted stent should not only inhibit thrombosis and promote endothelialization at an early stage but inhibit hyperplasia in the later stages of treatment.

Dopamine for coating of biomaterials has been extensively studied in the recent years. Dopamine can be grafted onto macromolecules to achieve greater stability, oxidation resistance, and adhesion [20]. The polycation chitosan and the polyanion hyaluronic acid have been proved that they are good biocompatibility materials used in endovascular [21]; hyaluronic acid is a physiological component of the extracellular matrix. Lee et al. grafted dopamine onto modified chitosan and hyaluronic acid, easily made an environmentally friendly film that can be used as a bag similar to polyvinyl one, and increased the mucoadhesion of high molecular weight chitosan [22–25]. Our group has previously reported a layer-by-layer self-assembled film with improved stability compared to unmodified film, and responsitivity to pH changes using the two dopamine-modified materials [26].

The microenvironment of the angioplasty site shows inflammation and is slightly acidic compared to normal tissue [1]. The pH-responsive layer-by-layer self-assembled coating was loaded with a drug. We suggested that this coating acts as in intelligent system to release the drug specifically in the acidic and inflammatory environment of the intervention.

In recent years, there has been more research on new drugs for application in drug-eluting stents. Statins, which are common clinical lipid-lowering drugs, are used in drug-eluting stents to eliminate atherosclerotic plaques [27]. They also provide an anti-inflammatory effect through the induction of autophagy at the site of atherosclerosis [28]. Besides synthetic drugs, enodgeneous mediators gain attention, because they integrate smoother in physiological regulation processes. NO is an endogenous gaseous signaling molecule that regulates vasodilation, controls smooth muscle cell proliferation, inhibits platelet aggregation and additionally exhibits antibacterial and anti-inflammatory functions [29]. The researchers prepared a catalyst on the scaffold [30], which can catalyze the release of NO to improve anticoagulation and prevent late restenosis of the stent.

H_2S is another gaseous signaling molecule that plays an important role in maintaining cerebral vascular homeostasis [31], protecting and regulating the central nervous system [32]. H_2S is used to promote angiogenesis [33] and anti-inflammatory mediators [34]. Similar to NO, high concentrations of H_2S are cytotoxic [35,36], but low concentrations are protective in the cardiovascular system. In contrast to NO, it does not form toxic peroxynitrite and other toxic degradation products [37,38]. H_2S can regulate the oxidative metabolism of low-density fatty acids [39], the vascular inflammatory response [40], vascular remodeling [41,42], and thrombosis [43] at atherosclerotic sites and in-stent restenosis. However, the dosage cannot be controlled by conventional injection or oral administration of H_2S. An exogenous H_2S donor as a drug would facilitate the application of this molecule for the treatment of cardiovascular diseases. Previous studies have shown the potential of the aspirin derivatives ACS14 and its metabolite ADTOH as H_2S donors [44]. ACS14 was shown to release H_2S, while maintaining the antithrombotic effects of aspirin. Our group synthesized this drug and loaded it into the coating on the surface of stents and tested the release profile of the drug. We demonstrated that ACS14 had cytoprotective and anti-inflammatory capabilities and therefore suggest it for use in the field of cardiovascular intervention [45].

In this study, catechol-modified chitosan and catechol-modified hyaluronic acid formed a pH-responsive coating on the surface of dopamine-modified 316 L stainless steel by layer-by-layer self-assembly. Subsequently, we loaded the H_2S donor ACS14, into the coating. The pH response of the film, its ability to release the drug adjusted to the microenvironmental pH, the cytocompatibility, and the blood compatibility of the film were evaluated *in vitro*. The effect of ACS14 on the atherosclerotic site was further evaluated by *in vivo* implantation experiments. These results may indicate a new direction for the development of controlled drug release systems in cardiovascular disease interventional therapy and highlight the value of H_2S in the field of cardiovascular disease treatment.

2. Materials and methods

2.1. Materials

Chitosan (100–200 mPa s, > 95% deacetylated), 3, 4-Dihydroxyhydrocinnamic acid (DHPA, 98%), *N*-(3-Dimethylaminopropyl)-*N′*-ethylcarbodiimide hydrochloride (EDC, ≥ 98.0%), 2-Morpholinoethanesulfonic Acid (MES, 99%), Dopamine hydrochloride (DOPA), Trizma® base, *N*-hydroxysuccinimide (NHS, 98%), hyaluronic acid (1.2 million Da), phosphate-buffered saline (PBS, pH 7.4), concentrated hydrochloric acid (HCl), and sodium hydroxide (NaOH) were purchased from Sigma-Aldrich. 1 mol/L HCl and 5 mol/L NaOH solutions were prepared. Aspirin derivatives were synthesized from methyl anthranil trisulfide and acetyl salicyl chloride (ACS14)[43]. The process of preparation of catechol-modified chitosan and hyaluronic acid has been reported previously [26].

2.2. Preparation of drug-loaded LBL self-assembled film

ACS14 solutions at concentrations of 10 μmol/L, 100 μmol/L, and 1000 μmol/L were prepared with a mixture of DMSO and PBS. After dopamine deposition on the smooth surface of the 316 L stainless steel (diameter = 1.0 cm), it was immersed for 10 min each time in Catechol chitosan (C-CS) solution (1 mg/mL in Reverses Osmosis (RO) water), Catechol hyaluronic acid (C-HA) solution (1 mg/mL in RO water), and ACS14 solution, sequentially. Further, it was immersed in RO water for 2 min to remove loosely bound C-CS and C-HA. After 5 rounds of deposition in each solution, three types of self-assembled films were finally prepared with different concentrations of ACS14.

2.3. Water contact angle measurement

The static water contact angle (WCA) of different samples, including drug-loaded coating prepared using different concentrations of ACS14 and 316 L stainless steel, were measured using an OCA35 goniometer (Dataphysics, Germany) with a fixed droplet volume of 5 μL. For the accuracy of the results, all measurements were repeated at least 5 times with 3 parallel samples.

2.4. SEM imaging

We analyzed the uniformity and compactness of the film surface to understand its morphology. Self-assembled coatings prepared by ACS14 at concentrations of 0 μmol/L, 10 μmol/L, 100 μmol/L, and 1000 μmol/L were observed at 3000 × magnification by scanning electron microscopy.

2.5. XPS analysis of drug-loaded coatings

In order to confirm the successful preparation of the drug loading of

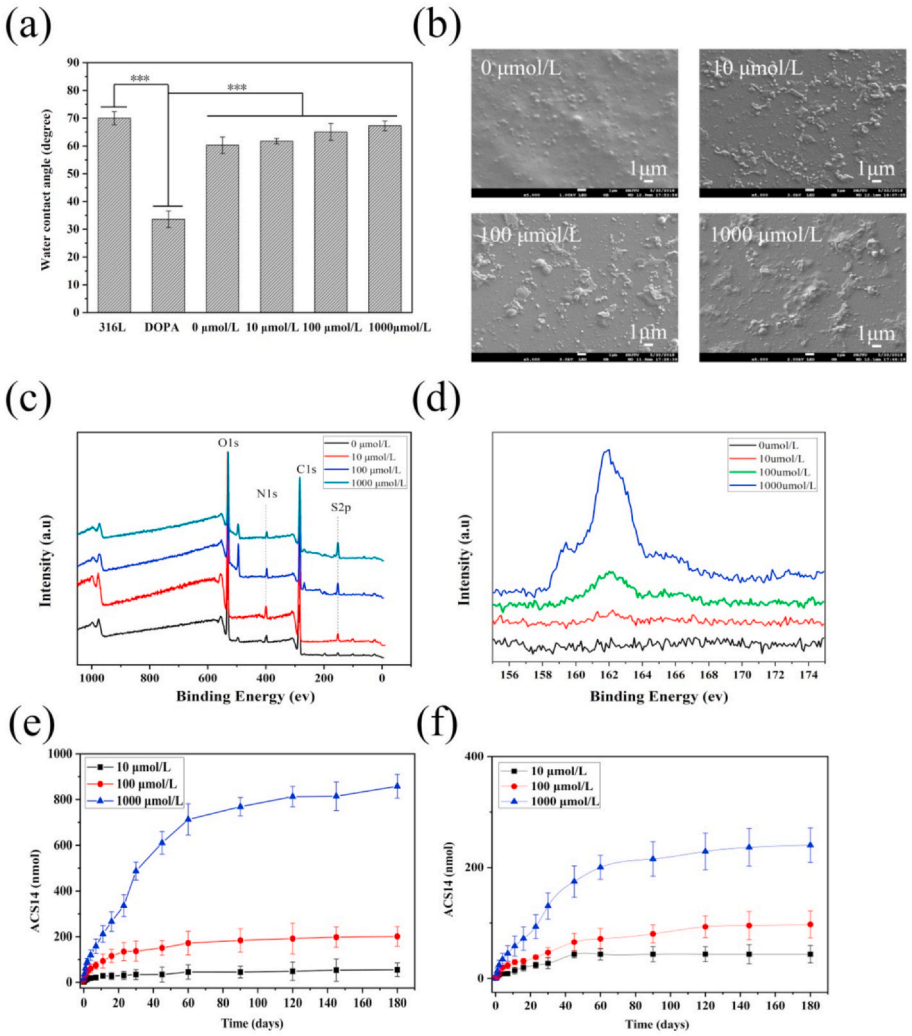

Fig. 1. (a) Water contact angle of different ACS14 concentration coatings (n = 5, ***p < 0.001). (b) SEM images of ACS14 coatings at different concentrations. (c) XPS full spectrum of drug-loaded coatings prepared with different concentrations of ACS14, and (d) high-resolution spectra of the S element content. (e) Drug release of the drug-loaded coatings in PBS at pH 6.5. (f) Drug release curve of drug-loaded coating in PBS at pH 7.4.

Table 1
The elemental content of the drug-loaded coating prepared by different concentrations of ACS14.

Sample (ACS14 μmol/L)	C (%)	N (%)	O (%)	S (%)
0	56.65	4.91	38.09	0.35
10	58.02	4.68	36.74	0.56
100	60.51	4.75	33.52	1.22
1000	62.64	4.25	31.29	1.82

the self-assembled film, the elements contained in the drug-loaded coatings prepared with different concentrations of ACS14 were quantified by X-ray photoelectron spectroscopy (PHI-5400, PerkinElmer, USA).

2.6. Drug release profiles of drug-loaded coatings prepared with different concentrations of ACS14 in PBS solution at different pH

The drug release profile of the layered self-assembled film prepared with ACS14 at concentrations of 10 μmol/L, 100 μmol/L, and 1000 μmol/L were tested in PBS solution at pH 6.5, and pH 7.4. Samples were placed in 15 mL PBS, and put into constant temperature shaker at 37 °C. 500 μL of the liquid was taken at 0.25, 0.5, 1, 2, 4, 7, 11, 16, 23, 30, 45, 60, 90, 120, 145, 180 days, measuring the absorbance at 460 nm using a microplate reader and comparing with a standard curve of defined concentrations, and 500 μL of the corresponding PBS solution was again added.

2.7. In vitro evaluation of platelet adhesion and activation

Fresh whole blood was obtained from the Blood Center of Chengdu, China. The samples were placed in 24-well cell culture plates. Further, 70 μL of platelet-rich plasma (PRP), which was obtained by centrifuging the blood samples at 1500 rpm for 15 min, was added to each sample. After incubating for 45 min at 37 °C in the incubator, the samples were washed with NaCl solution and then fixed with 2.5% glutaraldehyde. After staining with rhodamine, the samples were observed under a fluorescence microscope (Olympus, IX 51) to calculate the platelet adhesion area. The samples were gradually dehydrated and analyzed by SEM to observe the adhesion and activation level of the platelets.

2.8. In vitro evaluation of fibrinogen adhesion and its conformational changes

The samples were placed in a 24-well cell culture plate, and 70 μL of platelet-poor plasma (PPP) was added to each sample. After incubating for 1 h at 37 °C in the incubator, the samples were washed with PBS and blocked with 10 mg/mL bovine serum albumin (BSA) in PBS for 30 min.

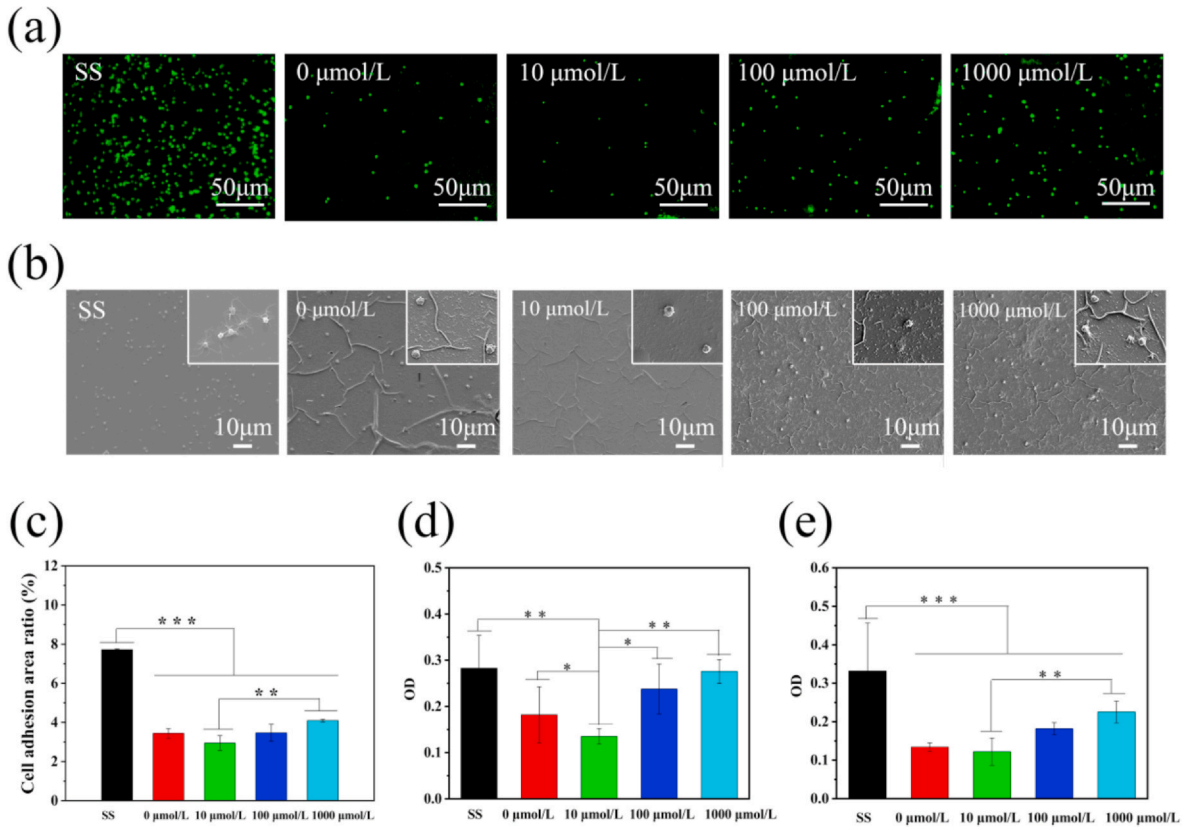

Fig. 2. (a) Fluorescence of platelets on the surface of samples prepared with different concentrations of ACS14, and (b) SEM morphology of platelets on the sample surface (n = 3, **p < 0.01, ***p < 0.001). (c) Platelet surface adhesion area of samples prepared with different concentrations of ACS14. (d) Fibrinogen denaturation. (e) Fibrinogen adhesion. (n = 3, *p < 0.05, **p < 0.01, ***p < 0.001).

After washing with PBS, 70 μL of antibody I (mouse anti-human fibrinogenγchain monoclonal antibody) and 70 μL of antibody II (HRP-labeled goat anti-rabbit polyclonal antibody) were added to the two sets of samples separately. The samples were detected by using ELISA kit (Hufeng Biotechnical Co., Shanghai, China).

2.9. Ex vivo blood circulation experiment to test for thrombogenicity

All procedures were performed in accordance with the Animal Protection Agreement of the China Animal Protection Association and Southwest Jiaotong University, and all ethical guidelines for experimental animals were followed. The experimental procedures were similar to those described [46]. The samples (1.2 cm × 1.0 cm) were rolled up and put into a heparinized polyvinyl chloride (PVC) circulation catheter with best possible attachment to the inner wall. After anaesthetizing the adult New Zealand white rabbits (approximately 3.0 kg), the left carotid artery and the right jugular vein of the rabbits were isolated. Further, the arteries and veins were connected to a PVC catheter to complete a blood circuit. After half an hour, the samples were removed from the animal and washed with NaCl solution. The samples were then photographed and weighed. Finally, they were observed with SEM, after being fixed in glutaraldehyde solution (2.5% in PBS) and dehydrated gradiently.

2.10. Cell growth on samples

Endothelial cells (ECs) and smooth muscle cells (SMCs) were isolated from human umbilical vessels. The umbilical cord was obtained with consent from a pregnant woman from the hospital. Macrophages were obtained from the abdomens of SD rats. ECs were cultured in DMEM/F12 supplemented with 15% FBS. SMCs were cultured in DMEM/F12 supplemented with 20% FBS. Macrophages were cultured in DMEM/F12 supplemented with 7% FBS.

The samples were placed in a 24-well cell culture plate, and 1 mL cell suspension (SMC, EC, and Macrophages) was added to each well. The densities of suspensions of SMC, EC, and Macrophages were 2×10^4 cells/mL, 8×10^3 cells/mL, and 3.5×10^4 cells/mL, respectively. CCK-8 was added to the 24-well cell culture plates after the cells were incubated for 4 h, 1 day, 3 days, and 5 days at 37 °C in a cell incubator with 5% CO_2. After the 4 h incubation, 150 μL of the cell culture medium of the 24-well cell culture plate was transferred into a 96-well cell culture plate, and the OD at 450 nm was measured with a microplate reader. Cell culture medium from Macrophages, incubated for various periods of time was tested for the expression of TNF-α and IL-10 using ELISA. Similarly, for cell culture medium of EC, NO release from EC was tested by Sievers 280i chemiluminescence NO analyzer (NOA 280i). The cells that were incubated for 4 h, 1 day, 3 days, and 5 days at 37 °C with 5% CO_2 in a 24-well cell culture plate, were washed with PBS (pH 7.4) and fixed with 2.5% glutaraldehyde. After staining with rhodamine, the samples were observed under a fluorescence microscope.

2.11. In vivo animal implantation experiment

Male Sprague-Dawley rats (n = 15, approximately 300 g) were used for this experiment. The samples were prepared through LBL self-assembly on 316 L wires, as described above. Briefly, the rats were anesthetized with pentobarbital sodium, and the samples were implanted into the lumen of the abdominal aortas. After 1 month, the samples were removed and fixed with 4% paraformaldehyde, and stained with Hematoxylin-Eosin (HE).

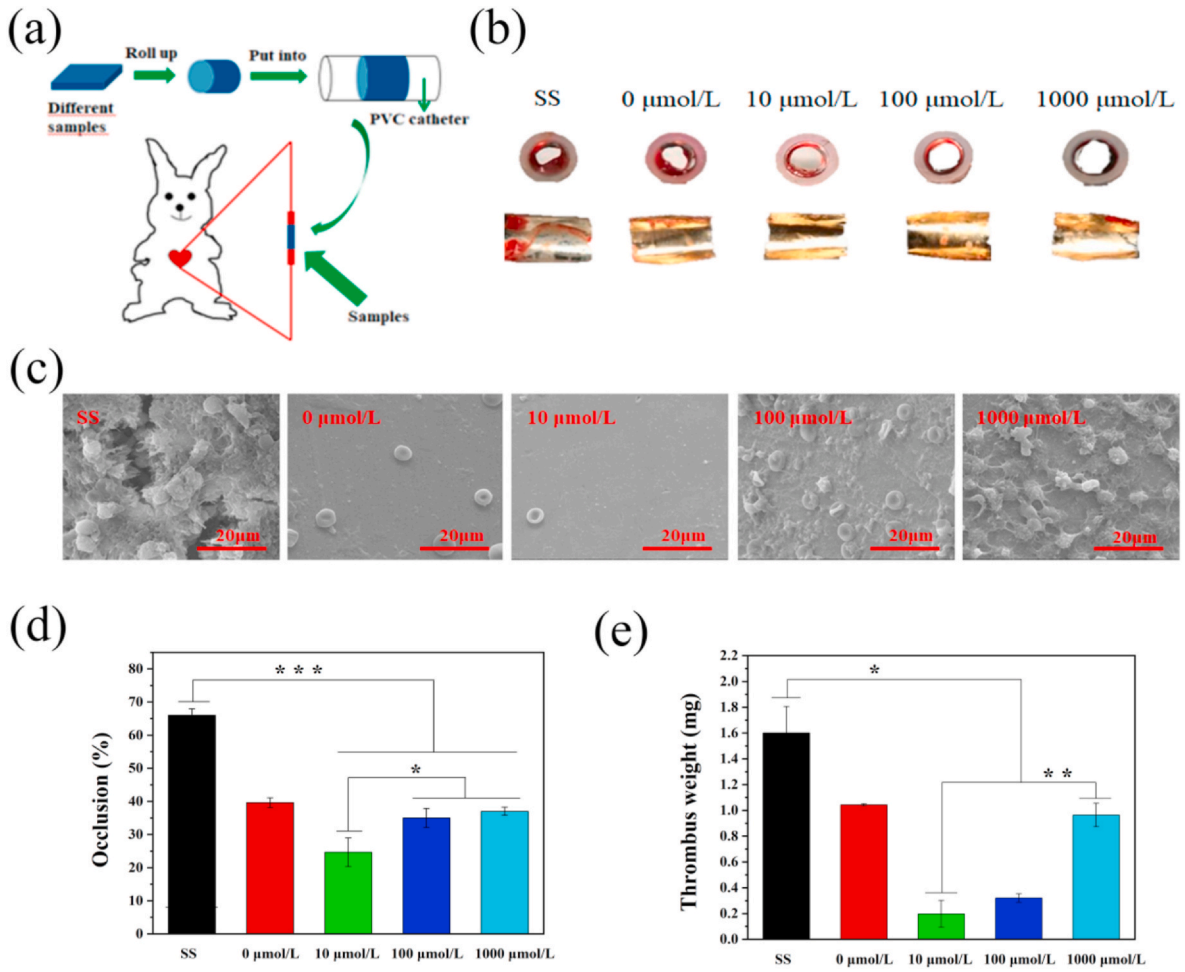

Fig. 3. (a) Schematic diagram of the experimental design. (b) The cross-section and inner views of different samples. (c) Coagulation of different samples observed with SEM. (d) Blood flow obstruction rate and (e) thrombus weight.(n = 3, *p < 0.05, **p < 0.01, ***p < 0.001).

2.12. Statistical analysis

All experiments were performed at least three times, and the results are expressed as mean ± standard deviation (SD). One-way analysis of variance (ANOVA) was used to analyze the experimental results, and the statistical difference between two groups was considered significant when $p < 0.05$.

3. Results and discussion

3.1. Preparation of pH-responsive drug-loaded coatings with different concentrations of ACS14

We previously demonstrated the pH-responsiveness of the chitosan-hyaluronic acid coating without drug loading by QCM-D [23]. In this study, the drug was loaded into the coatings, and the properties of the coatings were tested. Water contact angles of layer-by-layer self-assembled films with ACS14 at concentrations of 0, 10, 100, and 1000 μmol/L were observed, as shown in Fig. 1(a). The hydrophilicity of bare stainless steel and of the LBL coating was lower than that of the dopamine deposited stainless steel surfaces. ACS14 used in the drug-loaded coating caused a slightly dose-dependent increase of the water contact angles of the coating.

The surface topography of these coated samples was studied at 3000 × magnification, as shown in Fig. 1(b). The unloaded coating surface was relatively smooth and dense without any cracks. However, a few irregularly distributed protrusions of the surface with < 1 μm diameter were found, which may be due to the uneven distribution of dopamine and polyelectrolyte deposition during the assembly process. In contrast, the surface of the drug-loaded coating produced more convex deposits, and as the concentration increased, more substances bulged on the surface, indicating that the drug ACS14 was successfully loaded onto the coating, although it was probably not distributed homogeneously. To further confirm the result, the contents in the drug-loaded coating were detected by X-ray photoelectron spectroscopy, as shown in Fig. 1(c). The coatings prepared with different concentrations of ACS14 contained peaks of C1s, N1s, O1s, and S2p. The high-resolution spectrum of elemental sulfur (Fig. 1(d)) and the elemental content of each sample (Table 1) indicated that the amount of sulfur contained in the drug coating increased with increasing concentrations of ACS14. This increase was by 0.35%, 0.56%, 1.22%, and 1.82% in the coating, which shows that the coating was successfully loaded with different concentrations of the drug. Furthermore, we observed that the drug loading of the coating increased when a higher concentration of ACS14 was used in the preparation.

3.2. Drug release profile of self-assembled drug coatings

The coatings were immersed in PBS at pH 6.5 and pH 7.4 for 0, 0.25, 0.5, 1, 2, 4, 7, 11, 16, 23, 30, 45, 60, 90, 120, 145, and 180 days, and the drug release profile at 460 nm was measured using a microplate reader, as shown in Fig. 1(e and f). There was almost no burst release of the drug-loaded coating at both pH values, and the drug was mainly released during the first 60 days (the fastest release rate was between

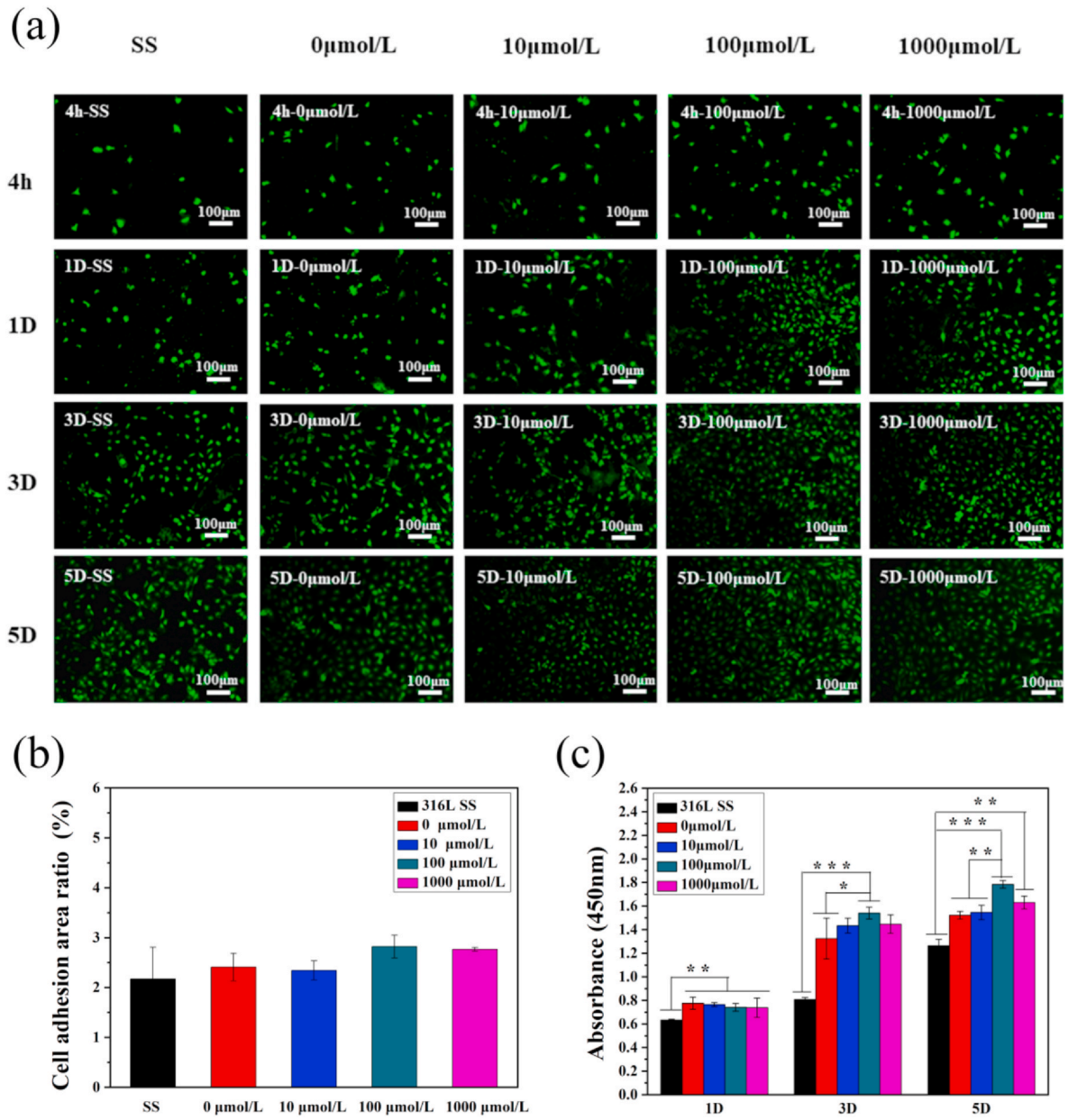

Fig. 4. (a) Fluorescence of endothelial cells growth after 4 h, 1D, 3D, 5D on different concentrations of drug-loaded coatings. (b) Adhesion area after 4 h of implantation on different samples. (c) CCK-8 testing endothelial cells viability map (n = 3, *p < 0.05, **p < 0.01, ***p < 0.001).

10 and 40 days). The drug release rate at pH 6.5 was higher than at pH 7.4. The pH dependence was more pronounced with increased ACS14 loading of the coating.

The drug release profiles indicated that the drug release was easier in a weakly acidic environment (pH 6.5) than at pH 7.4. This could be explained as follows: when the coating, which is in a balanced ionization state, is placed in an acidic environment at pH 6.5, providing an excess of H^+ ions in the surrounding solution, the equilibrium is disturbed, forming gaps between the macromolecules, releasing the drug. The pKa of chitosan in the coating material is 6.2, what changes the stability of self-assembled coating of chitosan and hyaluronic acid in a weakly acidic environment, and the degree of ionization is more severe, helping in drug release [47]. These results demonstrate the ability of the coating to release the drug triggered by the pH value in its microenvironment.

3.3. Evaluation of blood compatibility of the drug-loaded coatings

The drug-loaded coatings prepared at different concentrations of ACS14 were incubated with PRP for 45 min, and the platelets stained with rhodamine were observed under a fluorescence microscope at 400× magnification, as shown in Fig. 2(a). The platelet morphology on different drug-loaded coatings are shown in Fig. 2(b). Compared with the surface of the drug-loaded coatings, the aggregation and the amount of platelets on 316 L stainless steel were significantly higher. The platelets on stainless steel were mostly dendritic, which indicates high activation. Compared to the bare stainless steel surface, the platelet adhesion area on the coating without drug was significantly reduced, which means that the coating had a good ability to inhibit platelet activation and adhesion. The coating prepared with 10 μmol/L of ACS14 appeared useful concerning platelet adhesion. However, coatings prepared with 100 μmol/L and 1000 μmol/L ACS14 tended to promote platelet adhesion and activation. The opposite effect may be due to the varying concentrations of aspirin contained in ACS14 at the

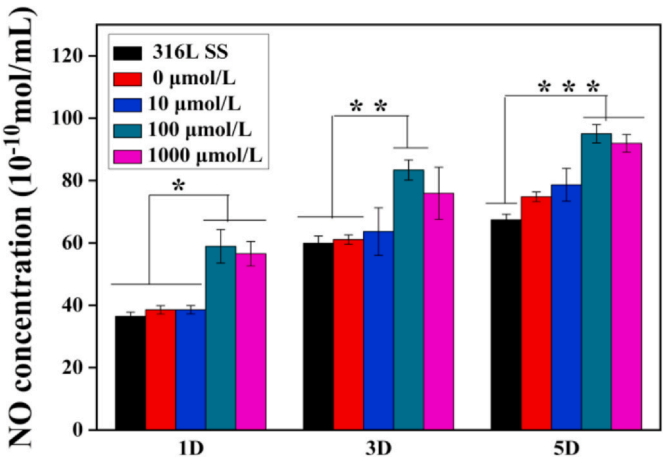

Fig. 5. Quantitative assessment of NO concentration in endothelial cell culture medium on different samples after culturing for 1, 3 and 5 days (n = 3, *p < 0.05, **p < 0.01, ***p < 0.001).

site of action. Aspirin has inhibits the formation of TXA2 and PGI2 [48 − 50]. TXA2 and PGI2 increase vascular smooth muscle contraction and platelet aggregation [51].

Blood coagulation can be affected by adhesion and denaturation of fibrinogen. The γ chain exposed by degenerated fibrinogen promotes platelet activation [52]. Therefore, the adhesion and denaturation of fibrinogen on the surface of the material is an important parameter for evaluating blood contact with materials. As shown in Fig. 2(d and e) The fibrinogen on the surface of the self-assembled coating was hardly denatured and adherent. The coating prepared with 10 μmol/L of ACS14 promoted the inhibitory effect, but excessive ACS14 (coating prepared with 100 μmol/L and 1000 μmol/L of ACS14) did not. The result was similar to that of platelet adhesion and activation.

3.4. Thrombogenicity test by ex vivo blood circulation

The ex vivo blood circulation test can intuitively illustrate the blood compatibility of the coatings, especially their anticoagulant ability. Fig. 3(a) shows the design of ex vivo blood circulation. The cross-sections and inner views of different samples after 30 min blood circulation in the arteriovenous shunt model are shown in Fig. 3(b). Coagulation on the bare stainless-steel surface was higher than on all of the coated surfaces. Further observation of the samples by SEM showed that there was thrombus formation on the surface of the bare stainless steel, whereas, the coating surface without the drug and the coating surface prepared by 10 μmol/L of ACS14 were almost free of red blood cells and platelets. Furthermore, there were some red blood cells and platelets adherent on the surface prepared by 100 μmol/L and 1000 μmol/L of ACS14, which is consistent with results of the platelet adhesion and fibrinogen denaturation assays. Quantitative analyses of blood flow obstruction rate (Fig. 3(d)), and thrombus weight (Fig. 3(e)) confirm this observation. These results show that layer-by-layer self-assembled coating and the coating prepared with 10 μmol/L of ACS14 had a better blood compatibility and did inhibit coagulation.

3.5. Cell culture experiment on the surface of the coating

The cytocompatibility of the coating is essential when it is in contact with the body vasculature. The coating should promote rapid endothelialization at the implant site for decreasing the occurrence of restenosis [53,54]. Thus, a drug-loaded coating in the interventional treatment of atherosclerosis should promote the adhesion and proliferation of endothelial cells and inhibit the proliferation of smooth muscle cells and macrophages [55].

Endothelial cells were seeded on the samples for 4 h, 1 day, 3 days, and 5 days. After staining with rhodamine, the morphology of the cells was observed with a fluorescence microscope (Fig. 4(a)), and it was observed that endothelial cells significantly increased with incubation time. The ECs on the surface presented typical cobblestone morphology. The surface of the sample containing the drug ACS14 had more endothelial cell growth than the drug-free coating and the bare stainless steel. However, the number of endothelial cells decreased when the drug concentration was too high. The number of cells on the materials after 2–4 h incubation in each group was comparable without significant difference after 4 h incubation, as shown in Fig. 4(b). The metabolic activity of the endothelial cells was measured by the CCK-8 test, and the cell proliferation curve was obtained. Fig. 4(c) shows that the coating prepared with 100 μmol/L ACS14 had the best effect of promoting endothelial cell proliferation. These two results show that the drug influences the proliferation of ECs, but has almost no significant effect on EC adhesion. This might be caused by H_2S regulating cystathionine b-synthase (CBS), which regulates vascular endothelial growth factor (VEGF), promoting EC proliferation [56].

In general, endothelial cells release signaling molecules such as NO, which have anticoagulant and anti-inflammatory effects and the ability to promote endothelial proliferation [35]. NO release was determined in the culture medium as shown in Fig. 5. The amount of NO released in the medium with 100 μmol/L ACS14 was the highest, indicating that the drug at this concentration acting on the endothelial cells promotes the largest release of NO by promoting endothelial cell proliferation. This is consistent with the activity and fluorescent imaging results of the endothelial cells which were highest on the surface of drug-loaded coatings prepared with 100 μmol/L of ACS14.

Activated macrophages release factors to accelerate the atherosclerotic inflammatory responses and thus, it is necessary to detect the proliferation and activation of macrophages on the surface of different samples. Stained with rhodamine, the surfaces of macrophages were observed under a fluorescence microscope, as shown in Fig. 6(a). The macrophages proliferated rapidly, and there was significant aggregation and cell rupture in 3 days. Fig. 6(b) displays the adhesion area of the macrophages after 4 h incubation on the surface of samples with different drug concentrations. The rhodamine fluorescence staining after 4 h incubation shows that the cells were uniformly distributed and the adhesion area was not significantly different between the groups. As shown in Fig. 6(c), the macrophages on the coating prepared with 100 μmol/L of ACS14 had the slowest proliferation rate, determined by CCK-8 assay, and low aggregation rate with mild rupture, indicating that this concentration of ACS14 inhibits the proliferation of macrophages. Although ACS14 inhibits the proliferation of macrophages, it has no significant effect on their adhesion. The ability of inhibiting proliferation of macrophages might be due to the anti-inflammatory effect of ACS14. *S*-diclofenac (ACS15), an H_2S donor, is proven to be anti-inflammatory [57].

Macrophages secrete a large number of cytokines in response to changes in the external environment, such as IL-1 and TNF-α, which are pro-inflammatory factors, and in later stages VEGF and IL-10, which are pro-recovery factors. These cytokines limit the inflammatory process and support tissue regeneration. Fig. 6(d–g) show the expression levels of TNF-α and IL-10 on the surface of samples with different concentrations of loaded drug. It can be seen that the expression levels of TNF-α was almost the same in day 1, except the sample prepared by 0 μmol/L. In day 3, the TNF-α expression on the surface prepared by 10 and 100 μmol/L ACS14 were higher than SS group and prepared by 0 μmol/L ACS14. The amount of IL-10 on the surface prepared with 1000 μmol/L ACS14 in day 1 was significant higher than that of other groups, indicating that higher concentrations of ACS14 inhibit the secretion of inflammatory factors and promotes more anti-inflammatory factors in short time. In day 3, the IL-10 expression on the surface of SS group and prepared by 0 μmol/L ACS14 were lower than other groups which also indicated ACS14 influenced the production of inflammatory factors, especially the samples prepared by 10 μmol/L ACS14. In day 5,

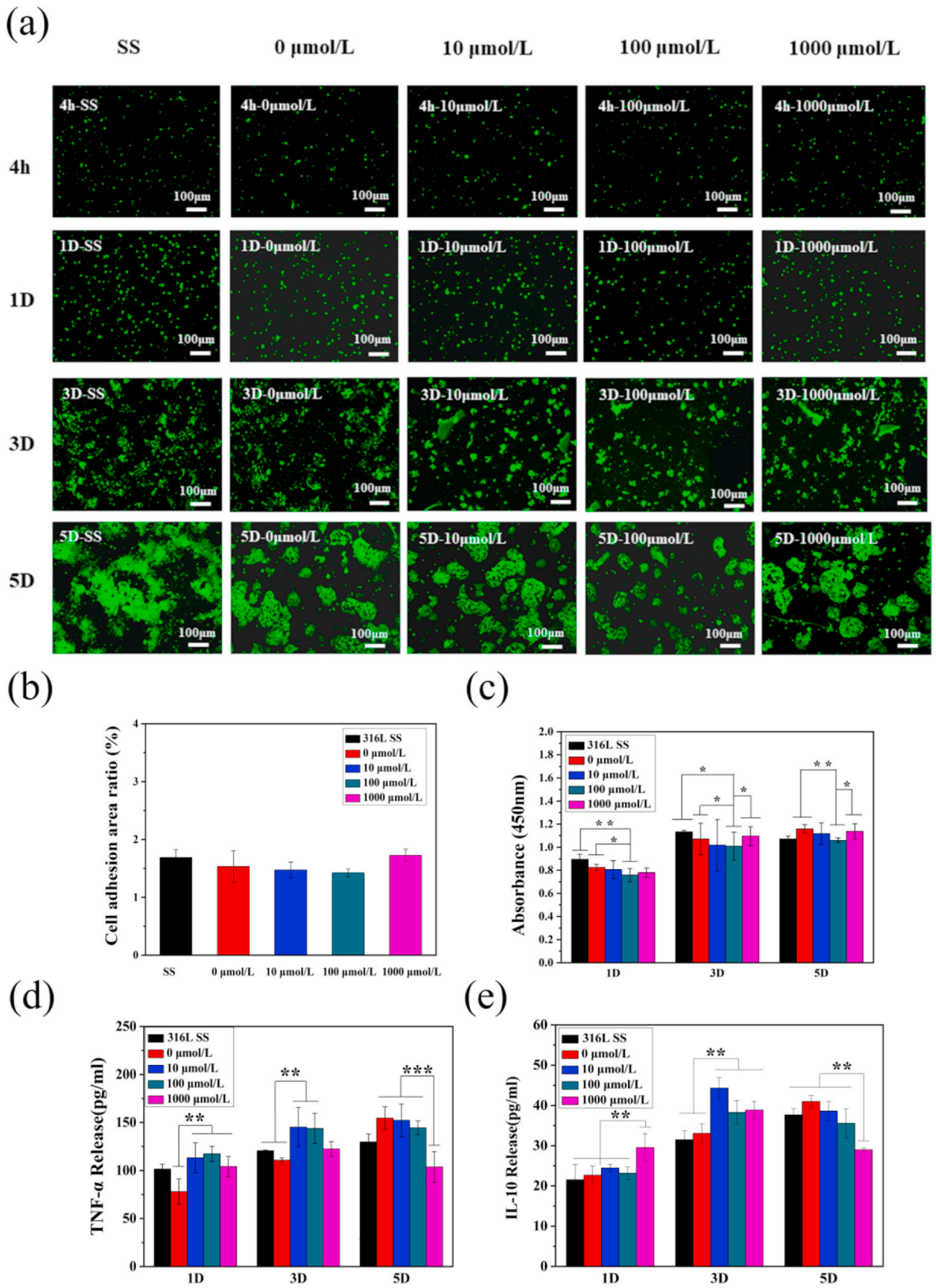

Fig. 6. (a) Fluorescence of macrophages after 4 h, 1D, 3D, and 5D on different samples. (b) Adhesion area of macrophages after 4 h of implantation on different samples, and (c) CCK-8 cells activity maps tested (n = 3, *p < 0.05, **p < 0.01). (d) ELISA kit detected the secretion of TNF-α from macrophages on different drug-coated surfaces, (e) ELISA kit detected the secretion of interleukin IL-10 on different drug-coated surfaces (n = 3, **p < 0.01, ***p < 0.001).

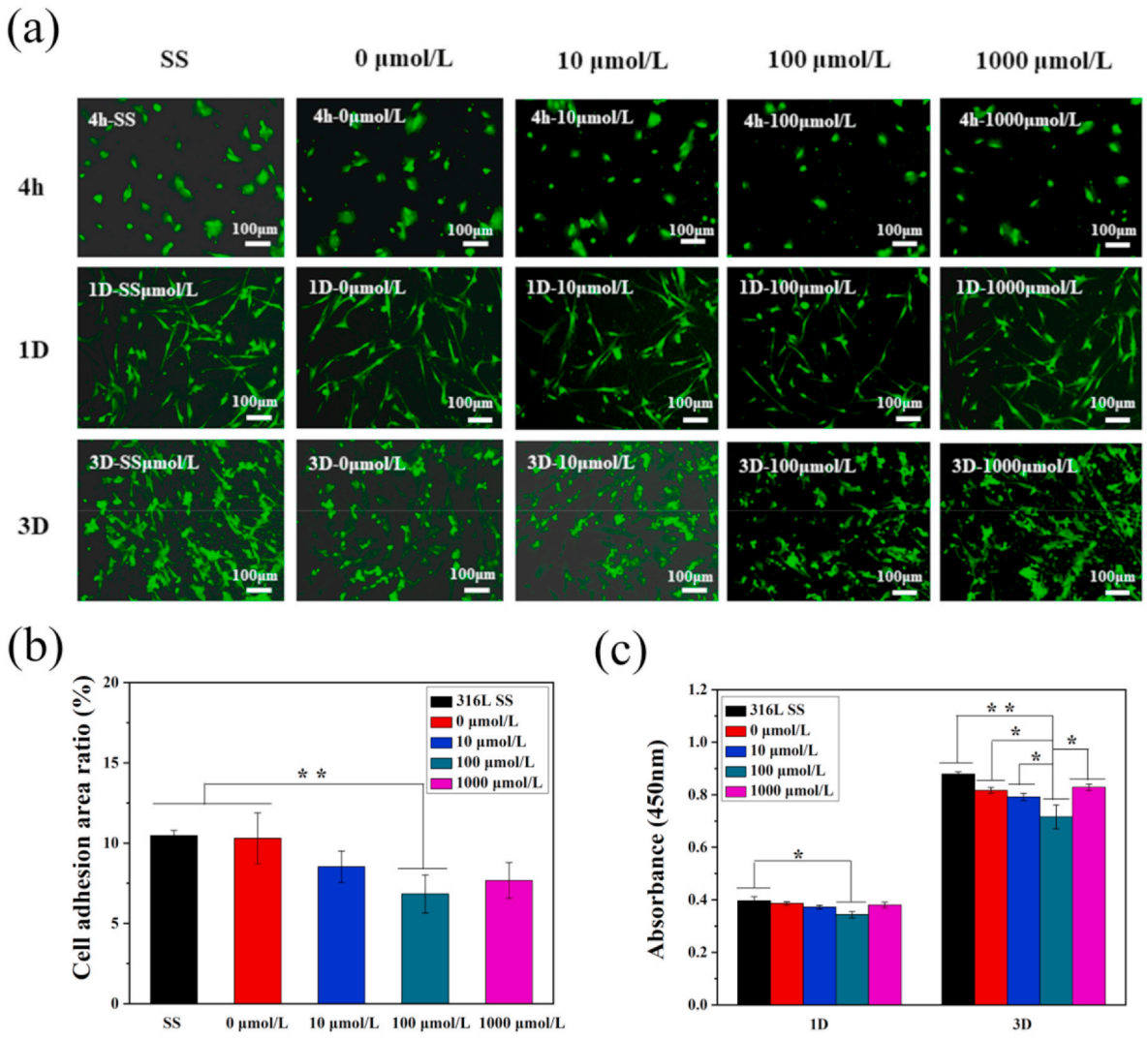

Fig. 7. (a) Fluorescence of smooth muscle cells after 4 h, 1D, 3D implantation on different concentrations of drug-loaded coatings. (b) Adhesion area of smooth muscle cells after 4 h of implantation on different samples, and (c) cells detected by CCK-8 activity map. (n = 3, *p < 0.05, **p < 0.01).

the TNF-α and IL-10 expression on the surface prepared by 1000 μmol/L ACS14 were obvious decreased. It might caused by the MA phenotype changing with time [58–60].

After implantation of the scaffold in the atherosclerotic region, smooth muscle cells proliferate and migrate easily, causing in-stent restenosis. Therefore, smooth muscle cells were cultured on the surface of the sample with varied incubation periods, and their activity and proliferation status were detected. The rhodamine stained smooth muscles were observed under a fluorescence microscope, as shown in Fig. 7(a). Smooth muscle cells proliferate rapidly with time. After three days, the morphology of the cells could change, due to excessive passaging or planting density. Fig. 7(b) shows the adhesion ability of smooth muscle cells after incubation for 4 h on the surfaces of different drug-loaded coatings. The number of smooth muscle cells on the surface of the drug-loaded coating prepared with 100 μmol/L ACS14 was lower when compared with the other groups. Furthermore, the number of smooth muscle cells on the surface of the drug-loaded coating was significantly lower than that on the surface of stainless steel. As shown in Fig. 7(c), ACS14 inhibited the growth of smooth muscle cells according to the CCK-8 assay. These results show that ACS14 inhibits the adhesion and proliferation of SMCs. This might be caused by H_2S, which inhibits VSMC proliferation by regulating mitochondrial fission [61]. It could also be due to the endogenous CSE or H_2S regulating the PLC-IP3 receptor and Ca^{2+}/Calmodulin signaling pathways, which further inhibits the proliferation of SMCs [62]. Some studies have reported that *S*-diclofenac (H_2S donor) inhibited rat vascular smooth muscle cell proliferation [63].

In summary, the cell compatibility of the drug-loaded coating prepared with 100 μmol/L ACS14 is the best choice to fit the required conditions.

3.6. In vivo animal implantation experiment

In order to further explore ACS14 and a novel coating for biomaterials for cardiovascular therapies, different concentrations of drug-loaded coated filaments were implanted into the abdominal aorta of SD rats. The surface was wrapped with neovascular tissue due to cell migration and adhesion after 30 days. After removing the sample, they were stained with HE. As shown in Fig. 8(a–f) The arteries at the implantation site of each sample were free of thrombus clogging. Additionally, the surface of the sample was covered with a layer of neointimal membrane, which was attached to the vessel wall. A deep layer was formed around the stainless steel and around samples with 0 μmol/L, and 10 μmol/L concentrations, which could be mainly caused by the inflammatory response of monocytes (macrophages).

The quantitative analysis is shown in Fig. 8(f). After the implantation of the bare stainless steel into the artery, smooth muscle hyperplasia was observed with an average area of the new tissue in the cross-

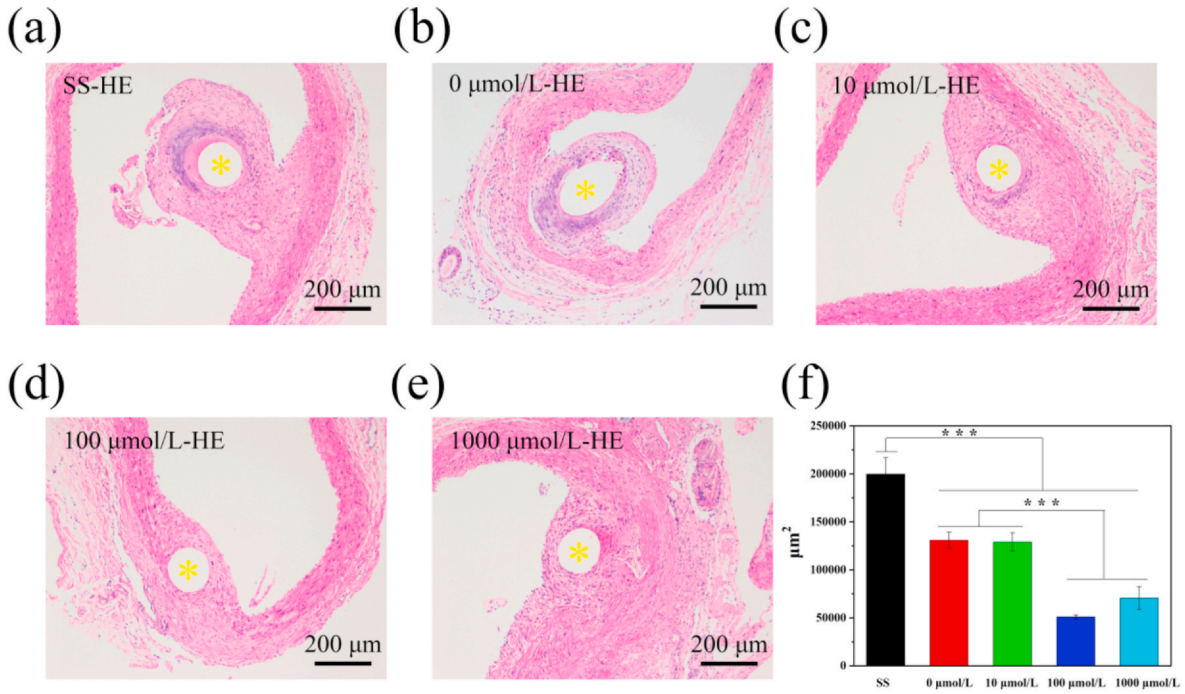

Fig. 8. Cross sections of aortae with bare and coated wires after four weeks implantation in rats. (a–e) HE histological images. (f) Quantitative analysis of tissue proliferation around the different samples, measured as cross-section areas (yellow* is the sample implantation position, n = 6, **p < 0.01,*p < 0.05).

section above 1.74 × 10^5 μm [2]. However, samples with 100 μmol/L and 1000 μmol/L ACS14 showed relatively thinner tissue area, approximately 0.63 × 10^5 μm [2] and 0.71 × 10^5 μm [2], respectively. The new tissue area of the sample prepared with the 100 μmol/L ACS14 was significantly smaller than that of the SS group and the coating group without drug. This indicates that at a certain concentration of ACS14, the proliferation of smooth muscle cells can be inhibited and, it might be due to H_2S or aspirin, which inhibits excessive proliferation of smooth muscle and reduces size of the new tissue [45,56].

4. Conclusion

In this study, we designed an intelligent, pH responsive, coating capable of releasing the gaseous mediator H_2S. The film was prepared by self-assembly of catechol-modified chitosan and catechol-modified hyaluronic acid on the surface of dopamine-coated stainless steel. The coating was loaded with different concentrations of the aspirin derived H_2S donor ACS14. The film can intelligently release the drug in response to a weakly acidic environment. Moreover, the surface of the drug-loaded coating can inhibit platelet adhesion and activation, as well as fibrinogen adsorption and denaturation. At the same time, inhibiting the proliferation of smooth muscle cells and macrophages reduced the inflammatory response at the interventional site and promoted the formation of new blood vessels. We found a U-shaped response curve of fibrinogen adsorption, platelet adhesion, endothelial growth and smooth muscle cell suppression, depending on the loading concentration of ACS14 in the coating with an optimum at 10–100 μmol/l. The design of this intelligent coating provides a potential method for the rational use of drugs in cardiovascular interventional therapy, and H_2S acts as a gas signaling molecule for the treatment of atherosclerosis, in order to provide a novel mechanism to solve in-stent restenosis.

CRediT authorship contribution statement

Bingyang Lu: Writing - original draft, Data curation. **Xiao Han:** Data curation. **Ansha Zhao:** Conceptualization, Writing - review & editing. **Dan Luo:** Data curation. **Manfred F. Maitz:** Writing - review & editing. **Haohao Wang:** Conceptualization. **Ping Yang:** Conceptualization. **Nan Huang:** Conceptualization.

Declaration of competing interest

The authors declare that they have no known competing financial interests or personal relationships that could have appeared to influence the work reported in this paper.

Acknowledgments

This work was supported by the National Natural Science Foundation of China (NSFC 81771988), and Sichuan Science and Technology Program (No.20GJHZ0268).

References

[1] A. Rezvan, C.W. Ni, N. Alberts-Grill, H. Jo, Animal, in vitro , and ex vivo models of flow-dependent atherosclerosis: role of oxidative stress, antioxid, Redox Signaling 15 (5) (2011) 1433–1448.
[2] P. Urban, E.D. Benedetti, Thrombosis: the last frontier of coronary stenting? Lancet 369 (9562) (2007) 619–621.
[3] G. Dangas, B.E. Claessen, A. Caixeta, E. Sanidas, G.S. Mintz, R. Mehran, In-stent restenosis in the drug-eluting stent era, J. Am. Coll. Cardiol. 56 (23) (2010) 1897–1907.
[4] B. Lagerqvist, S. James, U. Stenestrand, J. Lindback, T. Nilsson, L. Wallentin, Long-Term outcomes with drug-eluting stents versus bare-metal stents in Sweden, N. Engl. J. Med. 356 (10) (2007) 1009–1019.
[5] I. Sheiban, G. Villata, M. Bollati, D. Sillano, M. Lotrionte, G. Biondizoccai, Next-generation drug-eluting stents in coronary artery disease: focus on everolimus-eluting stent (Xience V®), Vasc, Healthc. Risk Manag. 4 (1) (2008) 31–38.
[6] M. Lin, C.W. Lou, J. Lin, T.A. Lin, Y. Chen, J. Lin, Fabrication of a biodegradable multi-layered polyvinyl alcohol stent, Fibers Polym. 19 (8) (2018) 1596–1604.
[7] P.W. Serruys, J.A. Ormiston, Y. Onuma, E. Regar, N. Gonzalo, H.M. Garciagarcia, K. Nieman, N. Bruining, C. Dorange, K. Miquelhebert, A bioabsorbable everolimus-eluting coronary stent system (ABSORB): 2-year outcomes and results from multiple imaging methods, Lancet 373 (9667) (2009) 897–910.
[8] W.C. Rose, Taxol: a review of its preclinical in vivo antitumor activity, Anti Canc. Drugs 3 (4) (1992) 311–322.
[9] M. Markaki, N. Tavernarakis, Metabolic control by target of rapamycin and autophagy during ageing - a mini-review, Gerontology 59 (4) (2013) 340–348.
[10] H. Tamai, K. Igaki, E. Kyo, K. Kosuga, A. Kawashima, S. Matsui, H. Komori, T. Tsuji,

S. Motohara, H. Uehata, Initial and 6-month results of biodegradable poly-l-lactic acid coronary stents in humans, Circulation 102 (4) (2000) 399–404.
[11] F. Vogt, A. Stein, G. Rettemeier, N. Krott, R. Hoffmann, J.V. Dahl, A. Bosserhoff, W. Michaeli, P. Hanrath, C. Weber, Long-term assessment of a novel biodegradable paclitaxel-eluting coronary polylactide stent, Eur. Heart J. 25 (15) (2004) 1330–1340.
[12] E.H. Seo, K. Na, Polyurethane membrane with porous surface for controlled drug release in drug eluting stent, Biomater. Res. 18 (1) (2014) 15 15.
[13] K. Sternberg, S. Kramer, C. Nischan, N. Grabow, T. Langer, G. Hennighausen, K. Schmitz, In vitro study of drug-eluting stent coatings based on poly(l-lactide) incorporating cyclosporine A – drug release, polymer degradation and mechanical integrity, J. Mater. Sci. Mater. Med. 18 (7) (2007) 1423–1432.
[14] S.W. Liu, C. Weng, S. Wang, W. Wang, M. Wang, A bioabsorbable, degradable stent with a drug release system, BIOMED. ENG-APP. BAS. C. 30 (3) (2018) 1850021.
[15] S. Prabhu, S.F.A. Hossainy, Modeling of degradation and drug release from a biodegradable stent coating, J. Biomed. Mater. Res. 80 (3) (2007) 732–741.
[16] M. Chen, H. Tsai, C.T. Liu, S.F. Peng, W.Y. Lai, S. Chen, Y. Chang, H. Sung, A nanoscale drug-entrapment strategy for hydrogel-based systems for the delivery of poorly soluble drugs, Biomaterials 30 (11) (2009) 2102–2111.
[17] R. Du, Y. Wang, Y. Huang, Y. Zhao, D. Zhang, D. Du, Y. Zhang, Z. Li, S. Mcginty, G. Pontrelli, Design and testing of hydrophobic core/hydrophilic shell nano/micro particles for drug-eluting stent coating, NPG Asia Mater. 10 (7) (2018) 642–658.
[18] M.F. Maitz, U. Freudenberg, M.V. Tsurkan, M. Fischer, T. Beyrich, C. Werner, Bioresponsive polymer hydrogels homeostatically regulate blood coagulation, Nat. Commun. 4 (1) (2013) 2168 2168.
[19] M.F. Maitz, J. Zitzmann, J. Hanke, C. Renneberg, M.V. Tsurkan, C. Sperling, U. Freudenberg, C. Werner, Adaptive release of heparin from anticoagulant hydrogels triggered by different blood coagulation factors, Biomaterials 135 (2017) 53–61.
[20] D. Gan, T. Xu, W. Xing, X. Ge, L. Fang, K. Wang, F. Ren, X. Lu, Mussel-Inspired contact-active antibacterial hydrogel with high cell affinity, toughness, and recoverability, Adv. Funct. Mater. 29 (1) (2019) 1805964.
[21] B. Thierry, F.M. Winnik, Y. Merhi, J. Silver, M. Tabrizian, Bioactive coatings of endovascular stents based on polyelectrolyte multilayers, Biomacromolecules 4 (6) (2003) 1564–1571.
[22] K. Kim, J.H. Ryu, D.Y. Lee, H. Lee, Bio-inspired catechol conjugation converts water-insoluble chitosan into a highly water-soluble, adhesive chitosan derivative for hydrogels and LbL assembly, Biomater. Sci. 1 (7) (2013) 783–790.
[23] Y. Lee, H. Chung, S. Yeo, C. Ahn, H. Lee, P.B. Messersmith, T.G. Park, Thermo-sensitive, injectable, and tissue adhesive sol–gel transition hyaluronic acid/pluronic composite hydrogels prepared from bio-inspired catechol-thiol reaction, Soft Matter 6 (5) (2010) 977–983.
[24] J.H. Ryu, S. Jo, M. Koh, H. Lee, Bio-Inspired, water-soluble to insoluble self-conversion for flexible, biocompatible, transparent, catecholamine polysaccharide thin films, Adv. Funct. Mater. 24 (48) (2014) 7709–7716.
[25] K.R. Kim, K. Kim, J.H. Ryu, H. Lee, Chitosan-catechol: a polymer with long-lasting mucoadhesive properties, Biomaterials 52 (52) (2015) 161–170.
[26] B. Lu, D. Luo, A. Zhao, H. Wang, Y. Zhao, M.F. Maitz, P. Yang, N. Huang, pH responsive chitosan and hyaluronic acid layer by layer film for drug delivery applications, Prog. Org. Coating 135 (2019) 240–247.
[27] C. Ye, J. Wang, A. Zhao, D. He, M.F. Maitz, N. Zhou, N. Huang, Atorvastatin eluting coating for magnesium-based stents: control of degradation and endothelialization in a microfluidic assay and in vivo, Adv. Mater. Technol. (2020) 1900947.
[28] F. Han, Q. Xiao, S. Peng, X. Che, L. Jiang, Q. Shao, B. He, Atorvastatin ameliorates LPS-induced inflammatory response by autophagy via AKT/mTOR signaling pathway, J. Cell. Biochem. 119 (2) (2018) 1604–1615.
[29] A.W. Carpenter, M.H. Schoenfisch, Nitric oxide release: Part II. Therapeutic applications, Chem. Soc. Rev. 41 (10) (2012) 3742–3752.
[30] Q. Zhao, Y. Fan, Y. Zhang, J. Liu, W. Li, Y. Weng, Copper-Based SURMOFs for nitric oxide generation: hemocompatibility, vascular cell growth, and tissue response, ACS Appl. Mater. Interfaces 11 (8) (2019) 7872–7883.
[31] P. Narne, V. Pandey, P.B. Phanithi, Role of nitric oxide and hydrogen sulfide in ischemic stroke and the emergent epigenetic underpinnings, Mol. Neurobiol. 56 (3) (2019) 1749–1769.
[32] S.A. Karimi, N. Hosseinmardi, M. Janahmadi, M. Sayyah, R. Hajisoltani, The protective effect of hydrogen sulfide (H2S) on traumatic brain injury (TBI) induced memory deficits in rats, Brain Res. Bull. 134 (2017) 177–182.
[33] W. Lin, C. Huang, S. Lin, M. Li, Y. Chang, Y. Lin, W. Wan, P. Shih, H. Sung, In situ depot comprising phase-change materials that can sustainably release a gasotransmitter H2S to treat diabetic wounds, Biomaterials 145 (2017) 1–8.
[34] W. Lin, W. Pan, C. Liu, W. Huang, H. Song, K. Chang, M. Li, H. Sung, In situ self-spray coating system that can uniformly disperse a poorly water-soluble H2S donor on the colorectal surface to treat inflammatory bowel diseases, Biomaterials 182 (2018) 289–298.
[35] K. Kashfi, The dichotomous role of H2S in cancer cell biology? Déjà vu all over again, Biochem. Pharmacol. 149 (2018) 205–223.
[36] C. Szabo, C. Ransy, K. Modis, M. Andriamihaja, B. Murghes, C. Coletta, G. Olah, K. Yanagi, F. Bouillaud, Regulation of mitochondrial bioenergetic function by hydrogen sulfide. Part I. Biochemical and physiological mechanisms, Br. J. Pharmacol. 171 (8) (2014) 2099–2122.
[37] X. Yu, L. Cui, K. Wu, X. Zheng, F.S. Cayabyab, Z. Chen, C. Tang, Hydrogen sulfide as a potent cardiovascular protective agent, Clin. Chim. Acta 437 (2014) 78–87.
[38] D.J. Polhemus, D.J. Lefer, Emergence of hydrogen sulfide as an endogenous gaseous signaling molecule in cardiovascular disease, Circ. Res. 114 (4) (2014) 730–737.
[39] S. Xu, Z. Liu, P. Liu, Targeting hydrogen sulfide as a promising therapeutic strategy for atherosclerosis, Int. J. Cardiol. 172 (2) (2014) 313–317.
[40] G. Wang, W. Li, Q. Chen, Y. Jiang, X. Lu, X. Zhao, Hydrogen sulfide accelerates wound healing in diabetic rats, Int. J. Clin. Exp. Pathol. 8 (5) (2015) 5097–5104.
[41] B. Tao, W. Cai, Y. Zhu, H2S is a promoter of angiogenesis: identification of H2S "receptors" and its molecular switches in vascular endothelial cells, Handb. Exp. Pharmacol. 230 (2015) 137–152.
[42] D.J. Polhemus, K. Kondo, S. Bhushan, S.C. Bir, C.G. Kevil, T. Murohara, D.J. Lefer, J.W. Calvert, Hydrogen sulfide attenuates cardiac dysfunction after heart failure via induction of angiogenesis, Circ. Heart Fail. 6 (5) (2013) 1077–1086.
[43] B. Olas, Hydrogen sulfide in hemostasis: friend or foe? Chem. Biol. Interact. 217 (2014) 49–56.
[44] A. Sparatore, E. Perrino, V. Tazzari, D. Giustarini, R. Rossi, G. Rossoni, K. Erdman, H. Schroder, P.D. Soldato, Pharmacological profile of a novel H2S-releasing aspirin, Free Radical Biol. Med. 46 (5) (2009) 586–592.
[45] A. Zhao, D. Zou, H. Wang, X. Han, P. Yang, N. Huang, Hydrogen sulphide-releasing aspirin enhances cell capabilities of anti-oxidative lesions and anti-inflammation, Med. Gas Res. 9 (3) (2019) 145.
[46] Z. Yang, Y. Yang, L. Zhang, K. Xiong, X. Li, F. Zhang, J. Wang, X. Zhao, N. Huang, Mussel-inspired catalytic selenocystamine-dopamine coatings for long-term generation of therapeutic gas on cardiovascular stents, Biomaterials 178 (2018) 1–10.
[47] Y. Chiu, M. Chen, C. Chen, P. Lee, F. Mi, U. Jeng, H. Chen, H. Sung, Rapidly in situ forming hydrophobically-modified chitosan hydrogels via pH-responsive nanostructure transformation†, Soft Matter 5 (5) (2009) 962–965.
[48] S. Jung, S. Lim, F. Albertorio, G. Kim, M.C. Gurau, R.D. Yang, M.A. Holden, P.S. Cremer, The vroman effect: a molecular level description of fibrinogen displacement, J. Am. Chem. Soc. 125 (42) (2003) 12782–12786.
[49] J.B. Smith, H. Araki, A.M. Lefer, Thromboxane A2, prostacyclin and aspirin: effects on vascular tone and platelet aggregation, Circulation 62 (1980) V19–V25.
[50] J.M. Ritter, Thromboxane and prostacyclin in platelet/blood vessel interaction: a commentary, in: C.T. Kappagoda, P.V. Greenwood (Eds.), Long-Term Management of Patients after Myocardial Infarction, Springer US, Boston, MA, 1988, pp. 233–244.
[51] J.M. Ritter, J.R. Cockcroft, H.S. Doktor, J. Beacham, S.E. Barrow, Differential effect of aspirin on thromboxane and prostaglandin biosynthesis in man, Br. J. Clin. Pharmacol. 28 (5) (1989) 573–579.
[52] G.A. Fitzgerald, M. Lupinetti, S.A. Charman, W.N. Charman, Presystemic acetylation of platelets by aspirin: reduction in rate of drug delivery to improve biochemical selectivity for thromboxane A2, J. Pharmacol. Exp. Therapeut. 259 (3) (1991) 1043–1049.
[53] J. Wang, B. Li, Z. Li, K. Ren, L. Jin, S. Zhang, H. Chang, Y. Sun, J. Ji, Electropolymerization of dopamine for surface modification of complex-shaped cardiovascular stents, Biomaterials 35 (27) (2014) 7679–7689.
[54] Y. Wei, Y. Ji, L. Xiao, Q. Lin, J. Xu, K. Ren, J. Ji, Surface engineering of cardiovascular stent with endothelial cell selectivity for in vivo re-endothelialisation, Biomaterials 34 (11) (2013) 2588–2599.
[55] T. Jiang, Z. Xie, F. Wu, J. Chen, Y. Liao, L. Liu, A. Zhao, J. Wu, P. Yang, N. Huang, Hyaluronic acid nanoparticle composite films confer favorable time-dependent biofunctions for vascular wound healing, ACS Biomater. Sci. Eng. 5 (4) (2019) 1833–1848.
[56] S. Saha, P.K. Chakraborty, X. Xiong, S.K.D. Dwivedi, S.B. Mustafi, N.R. Leigh, R. Ramchandran, P. Mukherjee, R. Bhattacharya, Cystathionine β-synthase regulates endothelial function via protein S-sulfhydration, Faseb. J. 30 (1) (2016) 441–456.
[57] L. Ling, G. Rossoni, A. Sparatore, C.L. Lin, P.D. Soldato, P.K. Moore, Anti-inflammatory and gastrointestinal effects of a novel diclofenac derivative, Free Radic. Biol. Med. 42 (5) (2007) 706–719.
[58] S.T. Eisenman, S.J. Gibbons, P.J. Verhulst, G. Cipriani, D. Saur, G. Farrugia, Tumor necrosis factor alpha derived from classically activated "M1" macrophages reduces interstitial cell of Cajal numbers, Neuro Gastroenterol. Motil. 29 (4) (2017).
[59] R.D. Malefyt, J. Abrams, B. Bennett, C.G. Figdor, J.E. Devries, INTERLEUKIN-10(IL-10) inhibits cytokine synthesis BY human monocytes - an autoregulatory role OF IL-10 produced BY monocytes, J. Exp. Med. 174 (5) (1991) 1209–1220.
[60] X. Wu, W. Xu, X. Feng, Y. He, X. Liu, Y. Gao, S. Yang, Z. Shao, C. Yang, Z. Ye, TNF-a mediated inflammatory macrophage polarization contributes to the pathogenesis of steroid-induced osteonecrosis in mice, Int. J. Immunopathol. Pharmacol. 28 (3) (2015) 351–361.
[61] A. Sun, Y. Wang, J. Liu, X. Yu, Y. Sun, F. Yang, S. Dong, J. Wu, Y. Zhao, C. Xu, Exogenous H2S modulates mitochondrial fusion–fission to inhibit vascular smooth muscle cell proliferation in a hyperglycemic state, Cell Biosci. 6 (1) (2016) 36 36.
[62] Y. Wang, X. Wang, X. Liang, J. Wu, S. Dong, H. Li, M. Jin, D. Sun, W. Zhang, X. Zhong, Inhibition of hydrogen sulfide on the proliferation of vascular smooth muscle cells involved in the modulation of calcium sensing receptor in high homocysteine, Exp. Cell Res. 347 (1) (2016) 184–191.
[63] R. Baskar, A. Sparatore, P.D. Soldato, P.K. Moore, Effect of S-diclofenac, a novel hydrogen sulfide releasing derivative inhibit rat vascular smooth muscle cell proliferation, Eur. J. Pharmacol. 594 (1) (2008) 1–8.